Aortic Regurgitation Dramatically Alters the Distribution of Atherosclerotic Lesions and Enhances Atherogenesis in Mice

Yu-Qing Zhou, Su-Ning Zhu, F. Stuart Foster, Myron I. Cybulsky and R. Mark Henkelman

Arterioscler Thromb Vasc Biol 2010;30;1181-1188; originally published online Mar 18, 2010;
DOI: 10.1161/ATVBAHA.110.204198
Arteriosclerosis, Thrombosis, and Vascular Biology is published by the American Heart Association. 7272 Greenville Avenue, Dallas, TX 72514
 Print ISSN: 1079-5642. Online ISSN: 1524-4636

Aortic Regurgitation Dramatically Alters the Distribution of Atherosclerotic Lesions and Enhances Atherogenesis in Mice

Yu-Qing Zhou, Su-Ning Zhu, F. Stuart Foster, Myron I. Cybulsky, R. Mark Henkelman

Objective—Hemodynamics plays a critical role in atherogenesis, but the association between flow pattern and preferential localization of lesion is not fully understood. We developed a mouse model of aortic valve regurgitation (AR) to change the aortic flow pattern and observed the effects on plaque formation.

Methods and Results—High-frequency Doppler ultrasound imaging of 10 untreated C57BL/6J mice and 6 sham-treated low-density lipoprotein receptor–deficient ($Ldlr^{-/-}$) mice revealed consistent antegrade blood flow throughout the aorta and oscillatory flow only along the lesser curvature of the aortic arch. Catheter-induced AR in 7 $Ldlr^{-/-}$ mice produced various degrees of diastolic retrograde flow throughout the aorta. After the mice were fed a cholesterol-enriched diet for 6 weeks, the burden of atherosclerotic lesions was increased 6-fold, with the naturally plaque-resistant descending aorta becoming susceptible. The AR severity correlated positively with the lesion burden in the descending thoracic and abdominal aorta but negatively with the lesions in the ascending aorta and aortic arch.

Conclusion—This AR model is valuable for elucidating the relationship between hemodynamics and predisposition of the artery wall to atherosclerosis, because of the significant alterations in local flow patterns and the conversion of large regions in the descending aorta from lesion resistant to lesion prone. **(*Arterioscler Thromb Vasc Biol*. 2010;30:1181-1188.)**

Key Words: atherosclerosis ■ blood flow ■ Doppler ultrasound ■ genetically altered mice

Complex and disturbed blood flow at sites of aortic curvature, branches, bifurcations, or other arterial regions is a predisposing factor for atherosclerosis.[1,2] Endothelial cells of arteries sense wall shear stress (WSS), the frictional force of blood flow, and respond differently to various flow patterns by triggering unique signal transduction pathways that lead to distinct gene expression patterns. Unidirectional laminar WSS diminishes endothelial inflammatory responses and protects the artery from atherosclerosis. In contrast, low time-averaged WSS with oscillating directions correlates with increased predisposition to atherosclerosis.[3,4] However, the association between flow dynamics and atherogenesis is still not fully understood, and the roles of low WSS and oscillatory WSS have never been differentiated. Useful insights have been gained from previous studies on animals of various species by altering the blood flow through a variety of surgical interventions.[4] However, those models focus on specific aspects of endothelial cell biology in limited vessel segments and are unable to provide, at the systemic level, an in vivo environment with flow alteration in a morphologically normal aortic system for a comprehensive elucidation of the flow-plaque relationship.

In the last decade, mice have commonly been used in biological research because this species is most amenable to genetic manipulation. Low-density lipoprotein receptor–deficient ($Ldlr^{-/-}$) and apolipoprotein E–deficient ($Apoe^{-/-}$) mice are the most popular strains for studies related to atherosclerosis.[5–9] A model was developed by placing a cast around the common carotid artery of $Apoe^{-/-}$ mice, in an attempt to induce 3 regions of lowered, increased, and oscillatory WSS.[10,11] The segment facing elevated WSS was spared from lesions. However, the proximal carotid artery exposed to the lowered flow velocity did not develop lesions evenly along the entire segment as one would expect if the low WSS was the key factor for plaque initiation. The flow pattern distal to the cast showed flow instability with associated vortices rather than oscillatory flow. As seen in humans, aortic valve regurgitation (AR) produces diastolic retrograde flow that extends to the distal aorta.[12,13] We reasoned that AR in mice would create oscillatory flow throughout the aorta and provide a novel model for exploring the effect of altered hemodynamics on atherogenesis.

High-frequency ultrasound imaging has been used to study cardiac morphology and flow dynamics in mice.[14–16] The entire curved flow path of the proximal aorta from aortic orifice to proximal descending aorta, including the lesser curvature, which is highly predisposed to atherosclerosis, can be visualized via the right parasternal window.[14] The abdom-

Received on: December 26, 2009; final version accepted on: March 4, 2010.

From Mouse Imaging Centre, The Hospital for Sick Children, Toronto, Ontario, Canada (Y.-Q.Z., R.M.H.); and Toronto General Research Institute and Department of Laboratory Medicine and Pathobiology (S.-N.Z., M.I.C.), Sunnybrook Health Sciences Centre (F.S.F.), and Department of Medical Biophysics (F.S.F., R.M.H.), University of Toronto, Toronto, Ontario, Canada.

Dr Zhou and Dr Zhu contributed equally to this work.

Correspondence to Yu-Qing Zhou, PhD, Toronto Centre for Phenogenomics, Mouse Imaging Centre, 25 Orde Street, Toronto, Ontario, Canada M5T 3H7. E-mail yqzhou@phenogenomics.ca

Arterioscler Thromb Vasc Biol **is available at http://atvb.ahajournals.org** **DOI: 10.1161/ATVBAHA.110.204198**

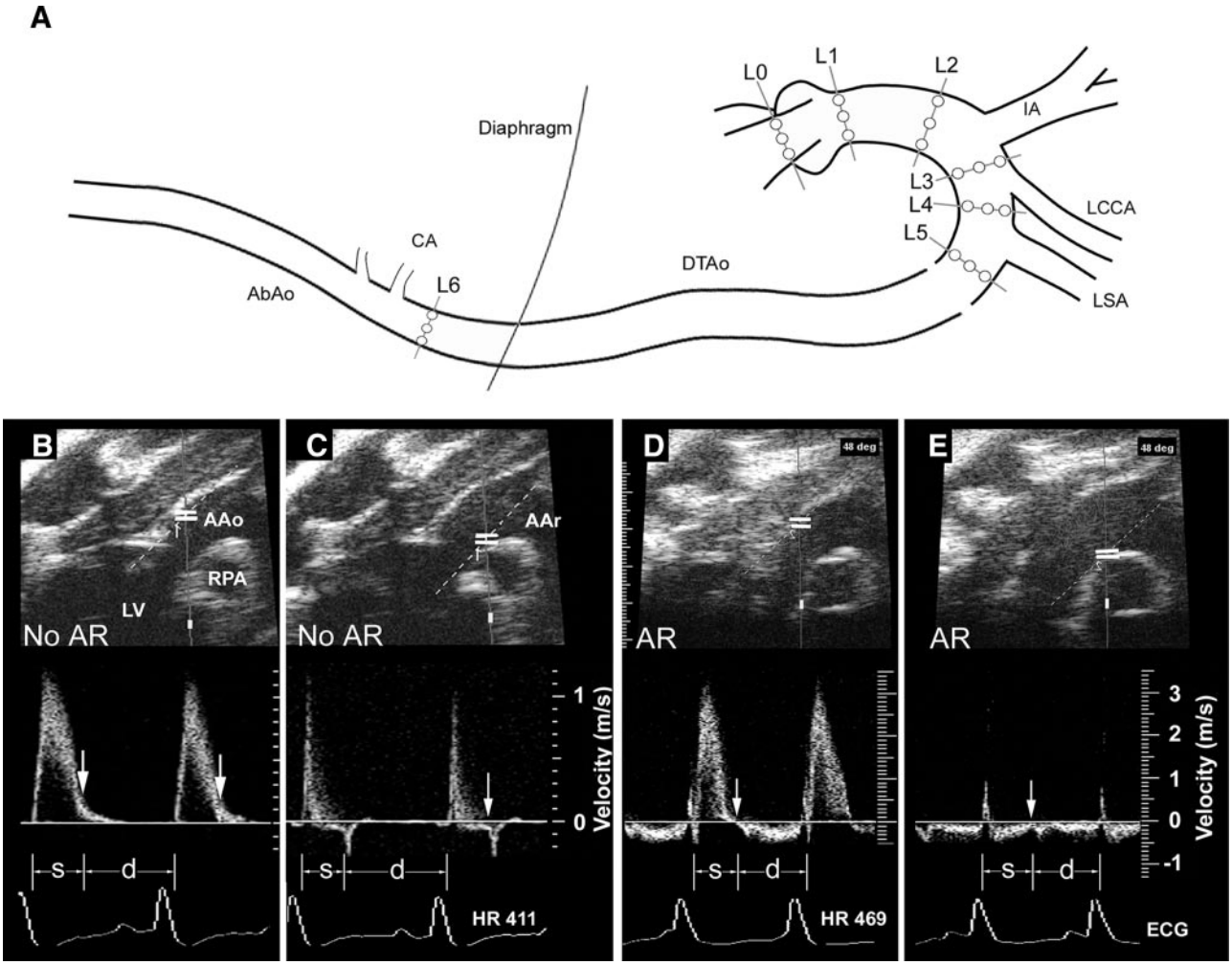

Figure 1. A diagram illustrating the location of pulsed Doppler flow measurements (open circles) in the aorta (A), and representative Doppler flow spectra (B through E). L0, aortic orifice; L1, proximal ascending aorta (AAo); L2, distal AAo; L3, aortic arch (AAr) distal to innominate artery (IA); L4, AAr distal to left common carotid artery (LCCA); L5, AAr distal to left subclavian artery (LSA); L6, the abdominal aorta (AbAo) proximal to celiac artery (CA). DTAo, descending thoracic aorta. Distinct Doppler flow spectra were found along the greater (B) and lesser (C) curvatures of the distal AAo (L2) in a normal C57BL/6J mouse and along the greater (D) and lesser (E) curvatures in an $Ldlr^{-/-}$ mouse with aortic regurgitation (AR). Arrows indicate the division between the systole (s) and diastole (d) (ie, the notch at the end of the descending branch of the flow waveform in B and the start of the negative spikes in C, D, and E).

inal aorta is also easily visualized. With pulsed wave Doppler and newly available Doppler color flow imaging,[17] the flow patterns in the mouse aorta can be comprehensively observed.

In this study, we evaluated aortic hemodynamics in C57BL/6J mice under baseline conditions and in $Ldlr^{-/-}$ mice with catheter-induced AR of different severity in comparison with their sham-treated counterparts. The effects of AR-induced oscillatory flow pattern on the extent and distribution of atherosclerotic lesions in $Ldlr^{-/-}$ mice were assessed. AR enhanced the overall lesion burden and dramatically altered plaque distribution, with increased plaques in the descending thoracic and abdominal aorta, regions that are naturally plaque resistant. Surprisingly, along the lesser curvature of the aortic arch, which is normally lesion prone, the plaque decreased with increasing AR severity.

Methods

Mice

Ten C57BL/6J mice were studied using pulsed Doppler for normal local flow patterns at 15 weeks of age (24.6±0.7g). Fifteen $Ldlr^{-/-}$ mice were used to study the effect of aortic flow alteration on the atherosclerotic distribution. In the experimental group of 8 $Ldlr^{-/-}$ mice, AR was created by catheterization via the right common carotid artery at 14 weeks of age. In the control group, with 7 $Ldlr^{-/-}$ mice of the same age, sham catheterization was conducted without damaging the aortic valve.

Creation of AR in $Ldlr^{-/-}$ Mice

Under anesthesia by ketamine hydrochloride (100 mg/kg) and xylazine (20 mg/kg), a plastic catheter was introduced via the right common carotid artery and forwarded to the aortic orifice under the guidance of ultrasound imaging. A metal wire was then introduced through the catheter to penetrate the noncoronary cusp of the aortic valve until Doppler recording showed significant diastolic retrograde flow in the aorta. At the end of surgical intervention, the catheter with the central metal wire was immediately withdrawn, and the right common carotid artery was ligated in both the AR group and the control group with sham catheterization. Temgesic (100 μL/20 gm) was given to reduce pain postsurgery.

Overall Experimental Protocol

In $Ldlr^{-/-}$ mice, pulsed Doppler measurements were made at 1 week postcatheterization in both the AR group and the control group.

These mice were then fed a defined semipurified 1.25% cholesterol high-fat diet (D12108, Research Diets, Inc.) for 6 weeks. Blood pressure was measured in $Ldlr^{-/-}$ mice before and 2 weeks after AR creation using a tail-cuff system, mainly for the systolic pressure because the diastolic pressure measured using this technique was less reliable. To confirm the persistence of flow alteration, the related Doppler flow parameters and the left ventricular dimensions and function were remeasured at 4 weeks of high-fat diet feeding in $Ldlr^{-/-}$ mice with AR. After 6 weeks of high-fat diet feeding, lesion area and distribution in $Ldlr^{-/-}$ mice were analyzed.

The experimental protocol was approved by the Animal Care Committee of the Hospital for Sick Children in Toronto, Ontario, Canada.

Observation of the Aortic Flow Pattern

A high-frequency ultrasound scanner (Vevo770, VisualSonics Inc., Toronto, Ontario, Canada) with a 30-MHz transducer was used. The related technical specifications, instrumental setting, and animal preparation have been described previously.[14] Following isoflurane anesthesia via a mask, Doppler flow spectra were recorded at 7 levels, as shown in Figure 1A. The Doppler sample volume was 115 μm laterally and $\leq$170 μm axially. At each level in the ascending aorta and aortic arch, Doppler recordings were made at 3 locations: (1) the region close to the greater curvature (outer radius), (2) the middle lumen, and (3) the region close to the lesser curvature (inner radius). In the proximal abdominal aorta, where a posterior curvature exists in the sagittal plane, the Doppler flow spectrum was recorded from the anterior (lesser curvature), middle, and posterior (greater curvature) parts of the lumen. A significant effort was made to reduce the potential effect of the intercept angle between Doppler beam line and flow direction on the flow velocity measurement. The transducer orientation was very carefully adjusted to make the Doppler intercept angle as small as possible, and all the velocity measurements were angle-corrected. In no measurement did the intercept angle exceed 60°.

C57BL/6J mice and the control $Ldlr^{-/-}$ mice without AR showed similar Doppler flow waveforms: (1) unidirectional biphasic pattern, with a major systolic antegrade waveform followed by a diastolic antegrade waveform of low velocity (Figure 1B); and (2) triphasic flow pattern, with an extra early diastolic retrograde wave (Figure 1C). By tracing the maximal velocity, the systolic antegrade time-velocity integral (TVI) and the diastolic retrograde and antegrade TVIs were measured separately.

In the $Ldlr^{-/-}$ mice with AR, biphasic Doppler waveforms were usually recorded, with antegrade flow during systole and retrograde flow throughout diastole (Figure 1D). At some locations along the lesser curvature of the aortic arch, the systolic antegrade flow waveform was very small, and the retrograde flow started to occur from the early systole (Figure 1E). In that situation, the systolic antegrade TVI and systolic retrograde TVI were measured separately. In comparing the Doppler flow parameters between the $Ldlr^{-/-}$ groups with and without AR, the total antegrade TVI during both the systole and diastole (ie, the whole cardiac cycle) and the total retrograde TVI during both the systole and diastole were used.

The diastolic retrograde TVI recorded at the center of the abdominal aorta was used to measure the overall AR severity. All parameters were averaged for 3 cardiac cycles.

In the supplemental experiments, the aortic flow pattern in C57BL/6J mice and in $Ldlr^{-/-}$ mice with and without AR was evaluated using Doppler color flow imaging, which visualizes the 2-dimensional flow distribution across the aortic lumen throughout cardiac cycle and provides further evidence for the local flow patterns observed by pulsed Doppler. In another group of C57BL/6J mice with and without AR, the aortic diameters and leukocyte count were measured.

Assessment of Atherosclerotic Lesion

After 6 weeks of high-fat diet feeding, blood was collected for measuring plasma cholesterol and white blood cells. Mice were perfusion-fixed with 4% paraformaldehyde. The entire aorta was harvested and stained with oil red O and cut into 3 segments: (1) the proximal aorta to the first pair of intercostal arteries, which was opened longitudinally along the greater curvature; (2) the descending thoracic aorta to the level of diaphragm; and (3) the abdominal aorta to its bifurcation. The descending thoracic aorta and abdominal aorta were opened along the frontmost wall. The aortic segments were pinned flat onto a black silicon dish for photography, and the relative surface area occupied by oil red O–stained lesions was quantified using software developed by Scion Co. (Frederick, Md). In this analysis, the proximal aortic segment was further divided to 3 regions: the ascending aorta from the distal margin of aortic sinuses to the level proximal to innominate artery, the proximal aortic arch proximal to the left subclavian artery, and the rest as the distal aortic arch.

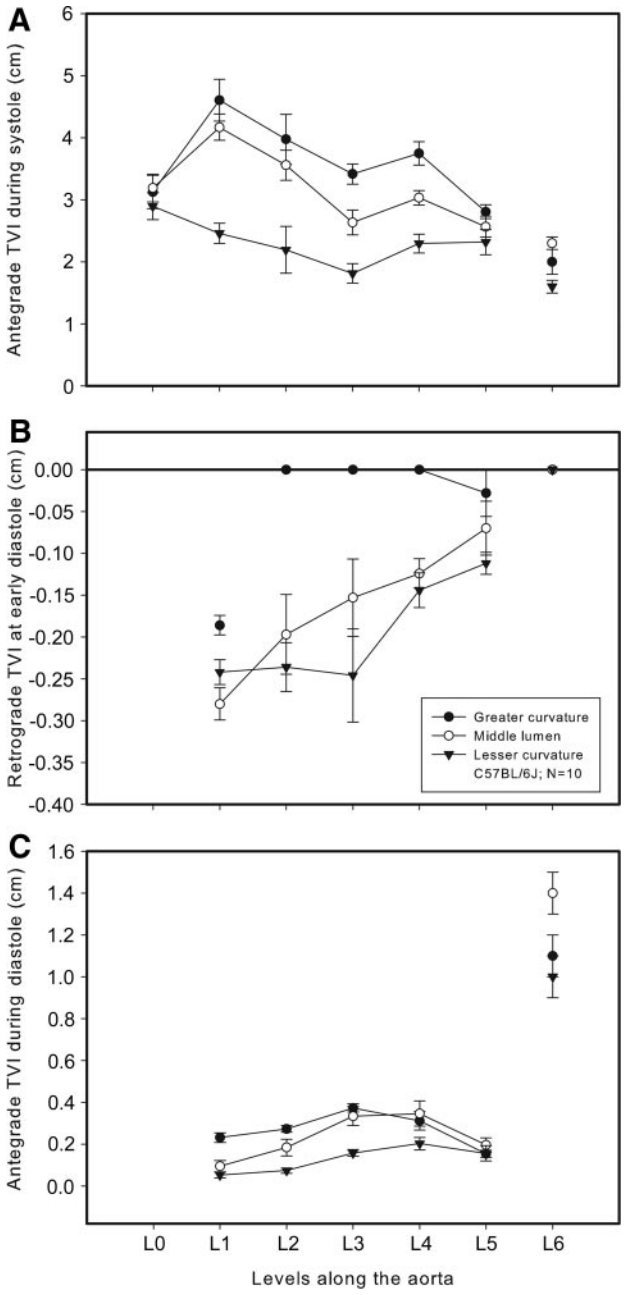

Figure 2. The systolic and diastolic TVIs of Doppler flow spectra across the aortic lumen measured at various levels along the aorta in 10 C57BL/6J mice. In the proximal abdominal aorta (L6), the greater curvature is located along the posterior wall and the lesser curvature along the anterior wall.

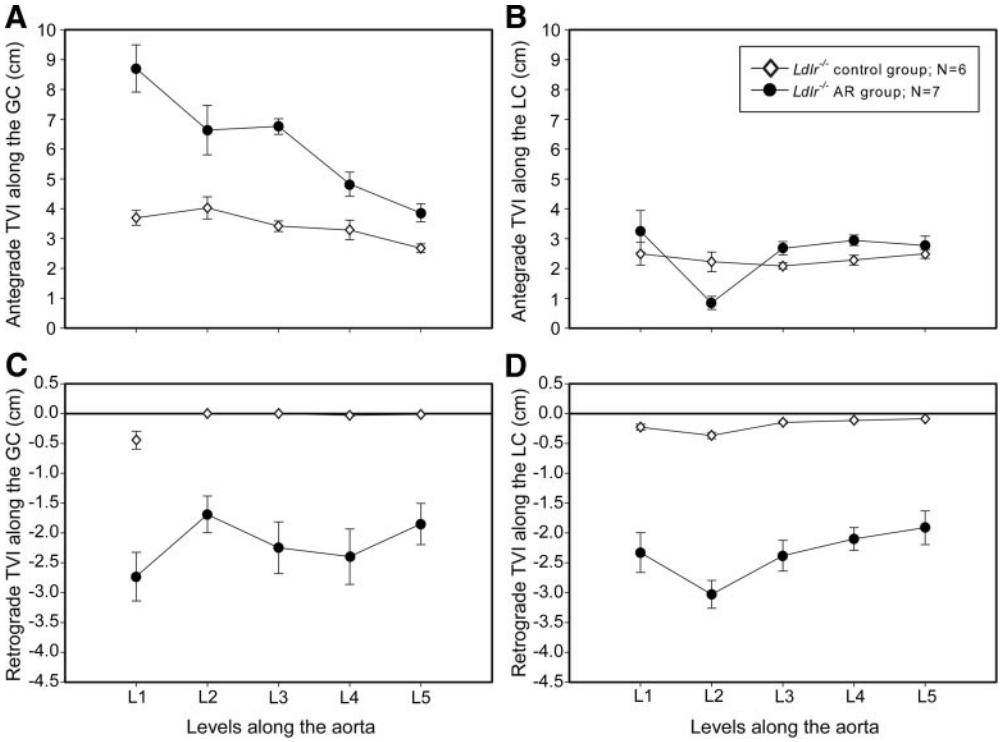

Figure 3. Antegrade and retrograde TVIs along the greater and lesser curvatures (GC and LC) of the ascending aorta and aortic arch (L1 to L5) in $Ldlr^{-/-}$ mice with AR are compared with those in $Ldlr^{-/-}$ mice without AR. The presented antegrade TVI is the sum of the antegrade TVIs in both systole and diastole. The retrograde TVI is the sum of the retrograde TVIs in both systole and diastole.

Statistics

All parameters were expressed as the mean±SEM. The Student *t* test was used to compare the plaque burdens between the $Ldlr^{-/-}$ mice with and without AR. Linear regression was used to evaluate the correlation between the AR severity and the plaque burden. $P<0.05$ was chosen as the level of statistical significance.

Results

The success rate of AR creation was higher than 90%. Only 1 AR mouse died from heart failure. One $Ldlr^{-/-}$ control mouse was excluded because of anatomic variations of the aorta.

Aortic Flow Pattern in C57BL/6J Mice

In the aortic orifice (L0), the velocity distribution was uniform across the lumen (Figure 2A). From the proximal ascending aorta to the distal aortic arch (L1 to L5), unidirectional biphasic flow spectrum was recorded along the greater curvature, with a major systolic antegrade waveform immediately followed by a diastolic antegrade wave of low velocity. In contrast, a triphasic or biphasic spectrum was found along the lesser curvature. A major systolic antegrade waveform was followed by a retrograde waveform at the early diastole and then by a small antegrade waveform or no flow in the rest of diastole (Figure 1B and 1C). Figure 2 shows the asymmetrical systolic antegrade flow with higher TVI along the greater curvature, the early diastolic retrograde flow detected mainly along the lesser curvature, and the mild antegrade flow in the rest of diastole between the proximal ascending aorta and the distal aortic arch. In the proximal abdominal aorta (L6), unidirectional biphasic flow waveform, with a major antegrade waveform during systole and a considerable antegrade waveform during diastole, was always found, with no retrograde flow throughout the cardiac cycle.

Altered Aortic Flow Pattern in $Ldlr^{-/-}$ Mice With AR

Control $Ldlr^{-/-}$ mice demonstrated a similar aortic flow pattern to that seen in C57BL/6J mice. In the $Ldlr^{-/-}$ mice with AR, the aortic flow pattern significantly changed, with diastolic retrograde flow occurring in the central aorta. In the ascending aorta and aortic arch, the systolic antegrade flow velocity along the greater curvature increased significantly (up to ≈3-fold) (Figure 1D) because of the compensation in left ventricular systolic function. In contrast, along the lesser curvature of the distal ascending aorta (L2), the systolic antegrade flow was significantly reduced in amplitude and also shortened in duration, appearing only during very early systole. As a consequence, the retrograde flow became much more temporally dominant, being present during the mid- to late systole and the whole diastole, especially in mice with severe AR (Figure 1E). Figure 3 compares the antegrade and retrograde TVIs along the greater and lesser curvatures of the ascending aorta and aortic arch (L1 to L5) between the $Ldlr^{-/-}$ groups with and without AR.

A biphasic flow pattern with diastolic retrograde flow was also observed in the proximal abdominal aorta (L6) of AR mice, which was not found in the control $Ldlr^{-/-}$ mice. A systolic antegrade flow with parabolic but slightly skewed velocity distribution was observed, with the velocity along the posterior wall (greater curvature) being significantly higher than that along the anterior wall (lesser curvature). The diastolic retrograde flow was symmetrically parabolic. In

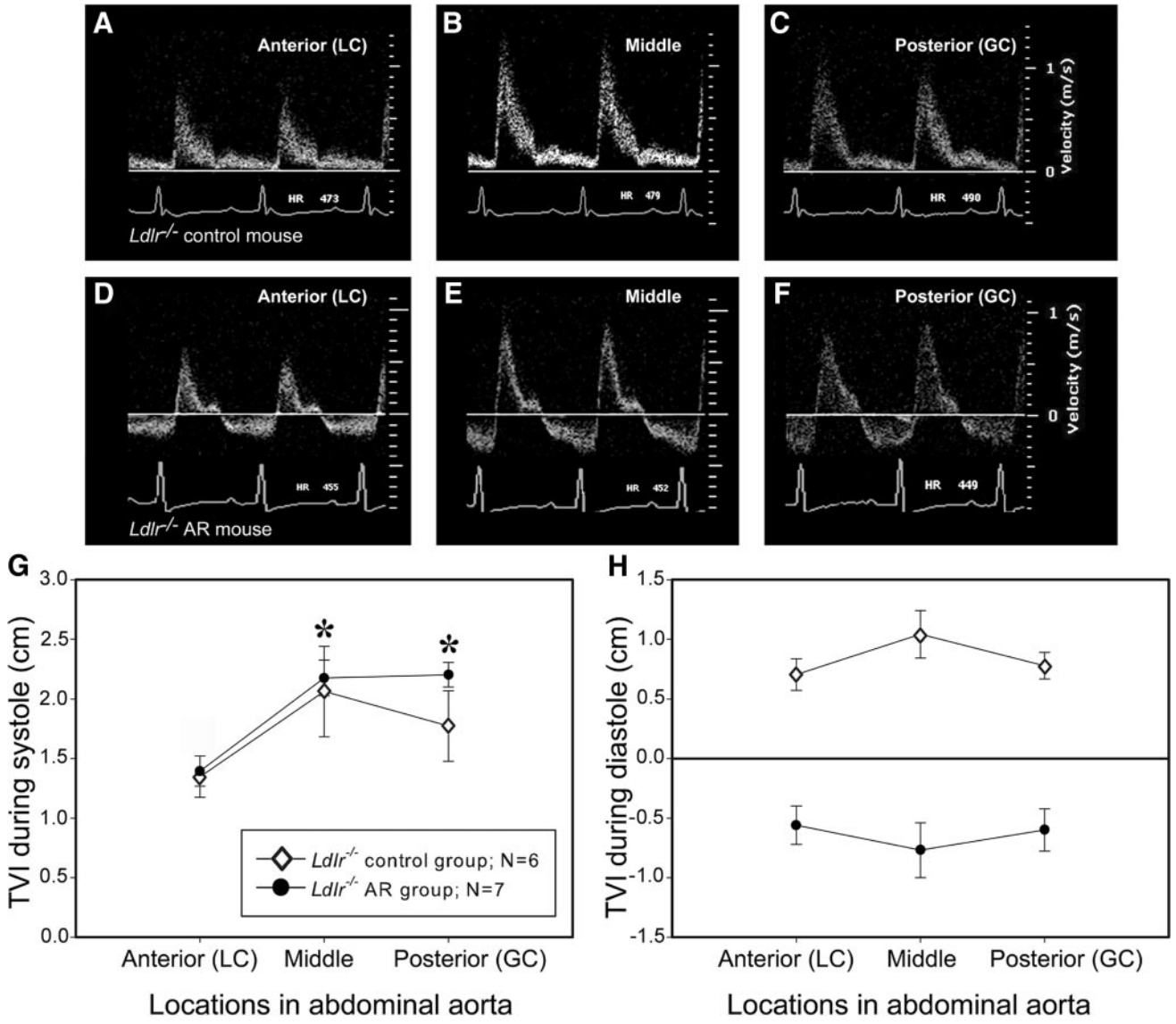

Figure 4. Comparison of Doppler flow spectra across the lumen of the proximal abdominal aorta obtained in *Ldlr*$^{-/-}$ mice without (A through C) and with (D through F) AR. GC indicates greater curvature; LC, lesser curvature. G, Systolic antegrade TVIs. **P*<0.05 compared with the corresponding value at the anterior wall only in AR group (by 2-way ANOVA). H, Diastolic TVIs of 2 groups.

terms of the Doppler spectral bandwidth, the flow spectrum in AR mice was similar to that in the *Ldlr*$^{-/-}$ control group, indicating laminar flow in both groups (Figure 4).

Compared with the *Ldlr*$^{-/-}$ control group, the AR group showed significant increases in the left ventricular chamber dimensions, wall thickness, stroke volume, and cardiac output at 1 week postcatheterization (Table). During 4 weeks of follow-up observation, the AR group showed further increases in the left ventricular chamber dimensions (the end-diastolic diameter increased from 4.3±0.1 to 4.7±0.2 mm, $P<0.05$; the end-systolic diameter increased from 3.0±0.1 to 3.5±0.2 mm, $P<0.05$) and in the posterior wall thickness at end-diastole (increased from 0.82±0.02 to 0.98±0.05 mm, $P<0.05$) but not in the left ventricular stroke volume (32.5±1.8 versus 34.8±3.5 μL) or the cardiac output (14.5±1.1 versus 16.0±2.4 mL/min). The severity of AR (measured as the TVI of the diastolic retrograde flow at the center of abdominal aorta) did not change over time (0.8±0.2 versus 0.9±0.2 cm). In *Ldlr*$^{-/-}$ mice with AR, the systolic blood pressure did not show any significant difference before and 2 weeks after AR induction (110±3 versus 109±2 mm Hg).

At the end of the study, the AR group displayed a significant increase in blood leukocyte count ($16.8\times10^6\pm1.8\times10^6$ versus $7.1\times10^6\pm0.8\times10^6$/mL, $P<0.01$) and in heart weight (0.18±0.04 versus 0.12±0.02 g, $P<0.05$), but no difference in body weight compared with the control group. There was no difference in serum cholesterol level between the AR and control groups (cholesterol, 30.3±1.7 versus 32.4±0.6 mmol/L).

Altered Distribution of Atherosclerosis in the *Ldlr*$^{-/-}$ Mice With AR

Lipid-laden lesions in the control *Ldlr*$^{-/-}$ mice were found primarily along the lesser curvature of the ascending aorta and proximal aortic arch, but not beyond the left subclavian artery (Figure 5A). The rest of the aorta was almost free of lesions, except for very small lesions at the ostia of branches.

Table. Cardiovascular Parameters of the *Ldlr*$^{-/-}$ Mice With and Without AR Determined 1 Week Postcatheterization (Mean±SEM)

Parameters	Control Group (n=6)	AR Group (n=7)
Body weight (g)	22.9±1.5	22.2±1.0
LV dimensions and function		
AWed (mm)	0.87±0.03	0.94±0.06
EDD (mm)	3.62±0.19	4.31±0.13*
PWed (mm)	0.72±0.02	0.82±0.02*
AWes (mm)	1.19±0.03	1.38±0.09
ESD (mm)	2.53±0.17	3.03±0.13*
PWes (mm)	1.02±0.03	1.10±0.06
Fractional shortening (%)	30.4±1.4	29.7±1.6
Ejection fraction (%)	66.1±2.1	64.9±2.5
Cardiac function by aortic Doppler flow		
Heart rate (bpm)	425±15	444±16
LV stroke volume (μL)	26.4±1.2	32.5±1.8*
Cardiac output (mL/min)	11.3±0.8	14.5±1.1*
Abdominal aortic flow (central)		
Systolic antegrade TVI (cm)	2.1±0.4	2.2±0.2
Diastolic TVI (cm)	1.0±0.2	−0.8±0.2*

AWed indicates anterior wall thickness at end-diastole; AWes, anterior wall thickness at end-systole; EDD, end-diastolic diameter; ESD, end-systolic diameter; PWed, posterior wall thickness at end-diastole; PWes, posterior wall thickness at end-systole; LV, left ventricle.

*$P<0.05$ compared with control group by the Student t test.

In *Ldlr*$^{-/-}$ mice with AR, the plaque burden of the whole aorta was significantly higher relative to the control group, largely because of a dramatic increase in lesions in the descending thoracic and abdominal aorta (Figure 5A and 5B). A positive correlation was found between plaque burden in the descending thoracic and abdominal aorta and the AR severity (Figure 5C). Moreover, the pattern of plaque distribution was closely related to the curvatures in the descending aorta, which mainly exist in the sagittal plane, as illustrated in Figure 1A. As seen from the dissected aortic specimen, plaques were always located along the lesser curvatures, which were the posterior wall of the midthoracic descending aorta and the anterior wall of the proximal abdominal aorta (Figure 5A).

In the ascending aorta and the proximal aortic arch, the plaque burden was comparable between the control and AR groups in terms of the average values. However, to our surprise, within the AR group the plaque burden along the lesser curvature tended to decrease with the increasing AR severity. Negative correlations ($r=0.81$ and ≈ 0.83; $P<0.05$) were found between the plaque burden in these 2 segments and the AR severity. In the distal aortic arch beyond the left subclavian artery, the plaque burden was significantly higher in the AR group than in the control group.

The Doppler color flow imaging in C57BL/6J mice and the *Ldlr*$^{-/-}$ mice with AR and the aortic diameter measurements and leukocyte count in C57BL/6J mice with AR are presented in the Supplemental Materials, available online at http://atvb.ahajournals.org.

Discussion

In this study, the aortic flow pattern in C57BL/6J mice serves as baseline physiological data for normal mice. The creation of AR in *Ldlr*$^{-/-}$ mice significantly alters the aortic flow pattern and fundamentally changes the atherosclerotic distribution in a consistent manner. To our knowledge, such a change in plaque distribution as a direct result of flow alteration has not been previously reported. The wide range of the changes in flow pattern and lesion severity enables a correlative analysis between the degree of oscillatory flow and the severity of plaque formation. We believe that this novel model with a controllable degree of flow alteration but no direct injury to the aortic wall is ideal for in-depth exploration of the interaction between the local flow dynamics and the aortic endothelium in early atherogenesis.

This study strongly suggests that oscillatory flow is a key factor in the initiation of atherosclerosis. First of all, in C57BL/6J and the *Ldlr*$^{-/-}$ mice without AR, the oscillatory flow pattern is observed only along the lesser curvature of the ascending aorta and the aortic arch, spatially corresponding to the predilection sites of plaques as found in this and previous studies.[8,9] Second, the present data confirm the consistent antegrade flow throughout cardiac cycle in the proximal abdominal aorta of normal mice, as was predicted by computational fluid simulations[18] and also observed in vivo by MRI.[19] Consistent with this, plaques are not abundant in the mouse abdominal aorta. This differs from the human abdominal aorta, which experiences significant diastolic flow reversal[2,20–22] and is a preferential site for plaque formation.[23] Furthermore, when AR was induced in *Ldlr*$^{-/-}$ mice, the descending thoracic aorta and abdominal aorta become plaque-prone. The only significant change in the Doppler flow recording was the presence of diastolic retrograde flow, whereas the systolic antegrade velocity and the properties of the flow spectrum (such as bandwidth) changed minimally.

Another possibility is that, even with the presence of oscillatory flow throughout the aorta, the elevated systolic antegrade velocity may be protective and prevent the aortic wall from developing plaque. As previously reported, endothelial cells subjected to elevated WSS tend to elongate and align in the direction of flow and undergo cytoskeletal remodeling. High WSS also promotes the release of vasodilators from endothelial cells that inhibit coagulation, adhesion, and migration of leukocytes and smooth muscle proliferation, while simultaneously promoting endothelial cell survival.[4] All these factors reduce the probability of plaque formation. In this study, the greater curvatures of the ascending aorta, the aortic arch, and other curved segments along the descending aorta facing the oscillatory flow pattern are spared from atherosclerotic lesions. The elevated systolic antegrade velocity at these locations may, to a certain extent, be responsible for the absence of plaque.

In mice with severe AR, plaques decrease significantly along the lesser curvature of the distal ascending aorta and proximal aortic arch, a region that is naturally prone to atherogenesis. A possible reason is that the dramatically

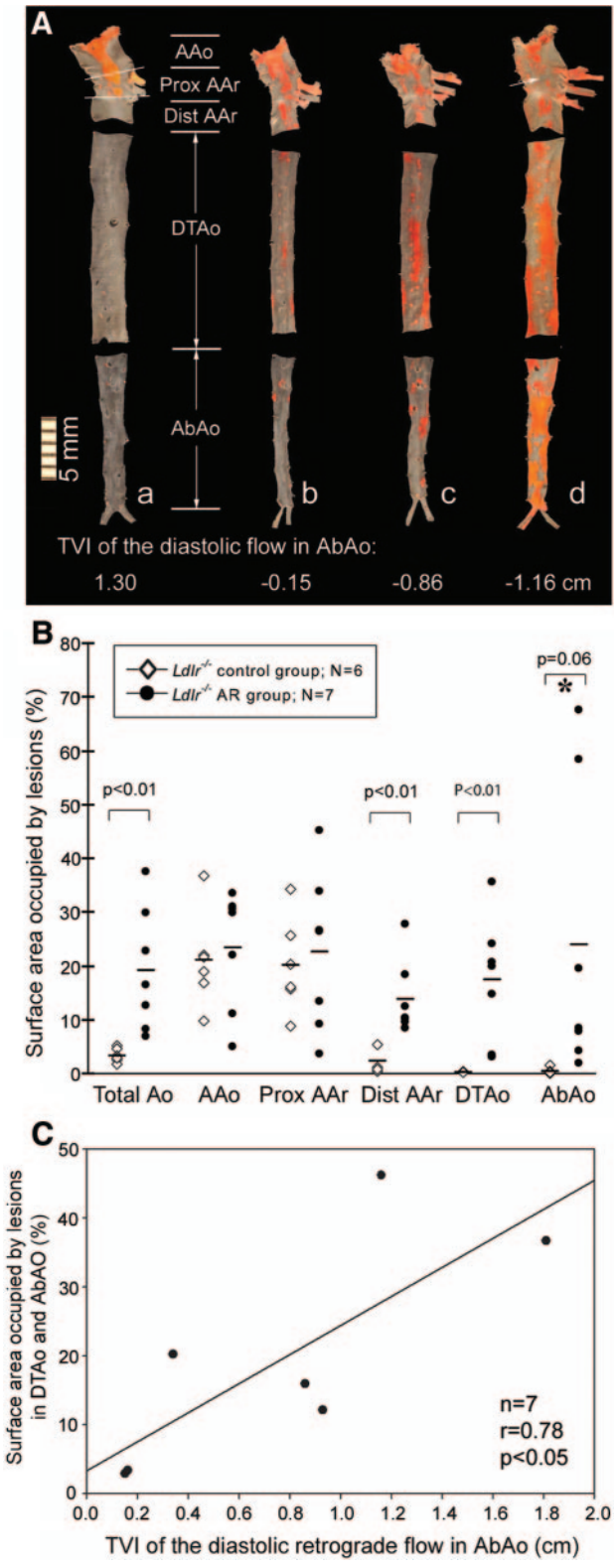

Figure 5. A, *En face* topography of oil red O–stained atherosclerotic lesions in the aorta of a typical control *Ldlr*$^{-/-}$ mouse without AR (a) and 3 *Ldlr*$^{-/-}$ mice with various degrees of AR (b through d). The arrow in d indicates a region with reduced lesion in the proximal aorta. The proximal aortic segment, which includes the ascending aorta (AAo), the proximal aortic arch (prox AAr), and the distal aortic arch (dist AAr), was cut along the greater curvature; thus, the lesions in the lesser curvature are found in the midline. The descending thoracic and abdominal aortic segments (DTAo and AbAo, respectively) were cut along the anterior wall, and the posterior wall is in the midline. B, The surface area occupied by lesions in different segments of the aorta was compared between groups of *Ldlr*$^{-/-}$ mice with and without AR. *$P<0.01$ by the Mann-Whitney rank sum test. C, The graph reveals a positive correlation between the plaque burden and the AR severity in DTAo and AbAo.

elevated antegrade flow velocity along the greater curvature causes a much more asymmetrical flow velocity distribution during systole, and consequently a very early flow reversal on the opposite side of the lumen because of flow separation. Thus, the flow pattern along the lesser curvature changes from oscillatory to predominantly retrograde. Similar flow separation and early reversal during systole along the lesser curvature was also observed in humans.[24]

AR may result in higher pulse blood pressure and to some extent promote plaque formation.[25] However, normal systolic blood pressure was observed in *Ldlr*$^{-/-}$ mice with AR, whereas the significant systolic expansion of the aorta with unchanged diastolic diameter was found in C57BL/6J mice with AR (Supplemental Table). We speculate that the pulse pressure in the AR mice studied did not significantly increase because of the normal compliance of the aorta in young adult mice as compared with the increased stiffness of the aorta in aged/hypertensive human patients.[25]

A number of systemic factors, such as heart failure and the consequent activation of the sympathetic nervous system and invocation of systemic mediators of inflammation, could contribute to the increased plaque formation. However, they would act in a systemic manner. The present data demonstrate a very distinctive, consistent, and nonuniform pattern of plaque redistribution in AR mice, with increased lesion burden in the descending aorta but comparable or decreased lesions in the ascending aorta and arch. These data strongly suggest a direct relationship between the AR-induced changes in local flow (associated with vascular morphology) and the lesion formation. In addition, the cardiac function in AR mice maintained a compensatory status during the experimental period, as evidenced by the normal left ventricular fractional shortening and the increased cardiac output. The fact that the leukocytosis was observed only in hypercholesterolemic *Ldlr*$^{-/-}$ mice with AR suggests a synergistic influence of the AR-induced flow alteration and the hypercholesterolemia on circulating leukocyte level. The enhanced atherogenesis with elevated circulating cytokines/growth factors may account for this.

Because of the limited acoustic window for ultrasound imaging, some aortic segments, such as most of the descending thoracic aorta, were not well visualized. For the accessible aortic segments, only a single imaging section was applied, and the flow pattern in 3-dimensional space was not demonstrated. However, the imaging section used in this study allowed visualization of the aortic arch with the most significant curvature. The plane with the most asymmetrical flow patterns and the aortic walls with the most asymmetrical plaque distribution were observed.

Only the axial flow velocity was measured, and the lateral flow could not be evaluated. Helical velocity has been described in the human aorta.[24] However, as seen from the

orientation of the plaques in mice, the flow in the axial direction plays the dominant role in plaque formation. The plaques are usually limited in a relatively narrow region in the axial direction, with little lateral extension.

With high-frequency ultrasound, this study convincingly demonstrates the spatial association between the local flow pattern and the atherosclerotic distribution in mice. In C57BL/6J and $Ldlr^{-/-}$ mice with unchanged flow dynamics, the oscillatory flow is found only along the lesser curvature of ascending aorta and aortic arch, corresponding to the plaque-prone region in $Ldlr^{-/-}$ mice. In the $Ldlr^{-/-}$ mice with catheter-induced AR, the oscillatory flow pattern is detected all over the central aorta, and the atherosclerotic distribution throughout the aorta is fundamentally changed. The descending thoracic and abdominal aorta, which normally face consistently antegrade flow and are naturally lesion-free, become plaque-prone, with the plaque burden positively correlated to the AR severity. However, even with the retrograde flow, the greater curvature of aorta, where the antegrade velocity is elevated, shows a decreased likelihood of developing plaques. This novel mouse model with wide variety of local flow patterns but no direct injury to arterial wall is ideal for studying the role of flow dynamics in atherogenesis in vivo at cellular and molecular levels.

Acknowledgments

The authors thank Dr S. Lee Adamson for the tail-cuff system for blood pressure measurement.

Sources of Funding

This work is part of the Mouse Imaging Centre at the Hospital for Sick Children and the University of Toronto. The infrastructure was funded by the Canada Foundation for Innovation and Ontario Innovation Trust. The research was funded by an Ontario Research and Development Challenge Fund, and the Heart and Stroke Foundation of Ontario (grants T6107 and T6060). Dr Henkelman and Dr Foster hold Canada Research Chairs. Dr Cybulsky is a Career Investigator of the Heart and Stroke Foundation of Ontario.

Disclosures

F.S.F. has a financial interest in VisualSonics Inc.

References

1. Ku DN, Giddens DP, Zarins CK, Glagov S. Pulsatile flow and atherosclerosis in the human carotid bifurcation: positive correlation between plaque location and low oscillating shear stress. *Arteriosclerosis*. 1985; 5:293–302.
2. Shaaban AM, Duerinckx AJ. Wall shear stress and early atherosclerosis: a review. *AJR Am J Roentgenol.* 2000;174:1657–1665.
3. Traub O, Berk BC. Laminar shear stress: mechanisms by which endothelial cells transduce an atheroprotective force. *Arterioscler Thromb Vasc Biol*. 1998;18:677–685.
4. Malek AM, Alper SL, Izumo S. Hemodynamic shear stress and its role in atherosclerosis. *J Am Med Assoc.* 1999;282:2035–2042.
5. Ishibashi S, Brown MS, Goldstein JL, Gerard RD, Hammer RE, Herz J. Hypercholesterolemia in low density lipoprotein receptor knockout mice and its reversal by adenovirus-mediated gene delivery. *J Clin Invest*. 1993;92:883–893.
6. Daugherty A. Mouse models of atherosclerosis. *Am J Med Sci*. 2002; 323:3–10.
7. Zadelaar S, Kleemann R, Verschuren L, de Vries-Van der Weij J, van der Hoorn J, Princen HM, Kooistra T. Mouse models for atherosclerosis and pharmaceutical modifiers. *Arterioscler Thromb Vasc Biol*. 2007;27: 1706–1721.
8. Cybulsky MI, Iiyama K, Li H, Zhu S, Chen M, Iiyama M, Davis V, Gutierrez-Ramos JC, Connelly PW, Milstone DS. A major role for VCAM-1, but not ICAM-1, in early atherosclerosis. *J Clin Invest*. 2001; 107:1255–1262.
9. Won D, Zhu SN, Chen M, Teichert AM, Fish JE, Matouk CC, Bonert M, Ojha M, Marsden PA, Cybulsky MI. Relative reduction of endothelial nitric-oxide synthase expression and transcription in atherosclerosis-prone regions of the mouse aorta and in an *in vitro* model of disturbed flow. *Am J Pathol*. 2007;171:1691–1704.
10. Cheng C, de Crom R, van Haperen R, Helderman F, Mousavi Gourabi B, van Damme LC, Kirschbaum SW, Slager CJ, van der Steen AF, Krams R. The role of shear stress in atherosclerosis: action through gene expression and inflammation? *Cell Biochem Biophys*. 2004;41:279–294.
11. Cheng C, Tempel D, van Haperen R, van der Baan A, Grosveld F, Daemen MJ, Krams R, de Crom R. Atherosclerotic lesion size and vulnerability are determined by patterns of fluid shear stress. *Circulation*. 2006;113:2744–2753.
12. Sutton DC, Kluger R, Ahmed SU, Reimold SC, Mark JB. Flow reversal in the descending aorta: a guide to intraoperative assessment of aortic regurgitation with transesophageal echocardiography. *J Thorac Cardiovasc Surg*. 1994;108:576–582.
13. Ambrosi P, Faugère G, Desfossez L, Habib G, Bory M, Luccioni R, Bernard P. Assessment of aortic regurgitation severity by magnetic resonance imaging of the thoracic aorta. *Eur Heart J*. 1995;16:406–409.
14. Zhou YQ, Foster FS, Nieman BJ, Davidson L, Chen XJ, Henkelman RM. Comprehensive transthoracic cardiac imaging in mice using ultrasound biomicroscopy with anatomical confirmation by magnetic resonance imaging. *Physiol Genomics*. 2004;18:232–244.
15. Stypmann J. Doppler ultrasound in mice. *Echocardiography*. 2007;24(1): 97–112.
16. Scherrer-Crosbie M, Thibault HB. Echocardiography in translational research: of mice and men. *J Am Soc Echocardiogr*. 2008;21:1083–1092.
17. Foster FS, Mehi J, Lukacs M, Hirson D, White C, Chaggares C, Needles A. A new 15–50 MHz array-based micro-ultrasound scanner for preclinical imaging. *Ultrasound Med Biol*. 2009;35:1700–1708.
18. Huo Y, Guo X, Kassab GS. The flow field along the entire length of mouse aorta and primary branches. *Ann Biomed Eng*. 2008;36:685–699.
19. Amirbekian S, Long RC Jr, Consolini MA, Suo J, Willett NJ, Fielden SW, Giddens DP, Taylor WR, Oshinski JN. In vivo assessment of blood flow patterns in abdominal aorta of mice with MRI: implications for AAA localization. *Am J Physiol Heart Circ Physiol*. 2009;297:H1290–H1295.
20. Oshinski JN, Ku DN, Mukundan S Jr, Loth F, Pettigrew RI. Determination of wall shear stress in the aorta with the use of MR phase velocity mapping. *J Magn Reson Imaging*. 1995;5:640–647.
21. Oyre S, Pedersen EM, Ringgaard S, Boesiger P, Paaske WP. In vivo wall shear stress measured by magnetic resonance velocity mapping in the normal human abdominal aorta. *Eur J Vasc Endovasc Surg.* 1997;13: 263–271.
22. Moore JE Jr, Maier SE, Ku DN, Boesiger P. Hemodynamics in the abdominal aorta: a comparison of *in vitro* and *in vivo* measurements. *J Appl Physiol*. 1994;76:1520–1527.
23. Holman RL, McGill HC Jr, Strong JP, Geer JC. The natural history of atherosclerosis: the early aortic lesions as seen in New Orleans in the middle of the 20th century. *Am J Pathol*. 1958;34:209–235.
24. Bogren HG, Mohiaddin RH, Kilner PJ, Jimenez-Borreguero LJ, Yang GZ, Firmin DN. Blood flow patterns in the thoracic aorta studied with three-directional MR velocity mapping: the effects of age and coronary artery disease. *J Magn Reson Imaging*. 1997;7:784–793.
25. Su TC, Chien KL, Jeng JS, Chang CJ, Hsu HC, Chen MF, Sung FC, Lee YT. Pulse pressure, aortic regurgitation and carotid atherosclerosis: a comparison between hypertensives and normotensives. *Int J Clin Pract*. 2006;60:134–140.

Aortic regurgitation dramatically alters the distribution of atherosclerotic lesions and enhances atherogenesis in mice

Yu-Qing Zhou[1], Su-Ning Zhu[2], F. Stuart Foster[3, 4], Myron I. Cybulsky[2], R. Mark Henkelman[1, 4]

[1]Mouse Imaging Centre, The Hospital for Sick Children, Toronto; [2]Toronto General Research Institute and Department of Laboratory Medicine and Pathobiology, University of Toronto; [3]Sunnybrook Health Sciences Centre; and [4]Department of Medical Biophysics, University of Toronto, Canada

Supplement Materials:

I. Confirmation of the aortic flow patterns using Doppler color flow imaging

(A) Aortic flow distribution in wild-type C57BL/6J mice

(B) Aortic flow distribution in *Ldlr*$^{-/-}$ mice with aortic regurgitation (AR)

II. Aortic diameter measurements and leukocyte count in C57BL/6J mice with AR

I. Confirmation of the aortic flow patterns using Doppler color flow imaging

By using high frequency pulsed Doppler ultrasound, the local aortic flow patterns have been evaluated in C57BL6/J mice and *Ldlr*$^{-/-}$ mice with and without aortic valve regurgitation (AR) and correlated with the atherosclerotic distribution and plaque burden. The data are presented in the primary paper. However, there are a few limitations in the technique used: (1) The location of pulsed Doppler sample volume in the aorta is less precise, especially when the aortic segments such as the ascending aorta move during the cardiac cycle. (2) Pulsed Doppler recordings from discrete locations do not directly delineate the overall flow velocity distribution across the aortic lumen. With the advent of the advanced high frequency Doppler color flow imaging technology with linear array transducer[(1)], it is feasible to visualize the flow velocity distribution across the aortic lumen in two-dimensional (2D) section. With an ECG-triggering function, consecutive Doppler color flow images can be obtained throughout the cardiac cycle. Such 2D Doppler color flow imaging with high spatial and temporal resolutions can further confirm the local flow patterns across the aortic lumen and their dynamic changes through the cardiac cycle as deduced from pulsed Doppler measurements. Moreover, color Doppler provides hemodynamic clues for explaining the asymmetrical velocity distribution and various local flow patterns such as the unidirectional and oscillatory flow waveforms observed using pulsed Doppler.

(A) Aortic flow distributions in wild-type C57BL/6J mice

Besides the system Vevo770, a new generation of high frequency ultrasound scanner Vevo2100 (VisualSonics Inc., Toronto) with a wide-band (18-38MHz) linear array transducer (the central frequency: 30MHz) was used. The spatial resolution of imaging is ~110μm (lateral) by ~50μm (axial). Doppler color flow imaging depicts the 2D overall flow distribution across the aortic lumen.

The frame rate can be up to 240fps when the color flow sampling window is reduced to the minimal (2.17mm wide). With ECG-triggering, consecutive color flow image frames can be obtained for every one milli-second throughout cardiac cycle[(1)].

Mice were prepared in the same way as described in the primary manuscript. In five C57BL/6J mice at 15 weeks of age, Doppler color flow imaging was conducted for the ascending aorta, aortic arch and abdominal aorta in the same imaging planes as for pulsed wave Doppler recording. The pulse repetition frequency was adjusted to a level which allowed aliasing to appear in the region with the highest velocity. With the smallest color Doppler sampling window but covering the region of interest and the optimal settings (high line density for color flow visualization), the effective frame rate obtained was about 70fps. The ECG triggering delay was initiated at the peak R wave, and increased in steps of 5ms for every consecutive frame. Consequently, 20~30 frames of Doppler color flow images were obtained throughout the entire cardiac cycle. The color flow frames at selected time points such as the peak systole, late systole to early diastole, and middle diastole were analyzed**.** The Doppler color flow imaging was qualitatively compared with the pulsed Doppler spectral recordings, in terms of the instantaneous flow direction, relative velocity amplitude across the lumen and dynamic change during the cardiac cycle.

It was found that, in the ascending aorta, the systolic flow moved forward with higher velocity along the greater curvature, and lower velocity along the lesser curvature **(Figure I-A, F)**. At early diastole, the flow along the lesser curvature reversed and moved to the aortic sinuses. A small reverse flow was also noticed along the greater curvature at the junction between the aortic sinuses and the proximal ascending aorta, but independent of the major flow downstream which continued to move forward along the greater curvature **(Figure I-B, G)**. This explains the early diastolic retrograde flow along the greater curvature at the level of proximal ascending aorta (but not beyond)

showed in **Figure 2B** in the primary manuscript. Following the closure of the aortic valves, the flow across the whole ascending aortic lumen either moved forward again at very low velocity or had no movement. The aortic arch had an asymmetrical velocity distribution generally similar to the distal ascending aorta, with highest velocity along the greater curvature during systole and a retrograde flow along the lesser curvature at early diastole **(Figure I-C, D, F, G)**. The findings with Doppler color flow imaging provide the hemodynamic evidence for the various local flow patterns at discrete locations as demonstrated by pulsed Doppler **(Figure I-H, I, J)**.

We speculate that the asymmetrical flow distribution and different local flow patterns across the aortic lumen in the ascending aorta and the aortic arch are caused by the off-axial entry of the inlet flow jet from the aortic orifice to the ascending aorta, the discrepancy in diameter between the aortic orifice and the proximal ascending aorta, and the continuously curved flow path downstream. Thanks to the high spatial resolution of high frequency ultrasound, the backscatter from the blood was visible in the 2D imaging. In the ten C57BL/6J mice presented in the primary manuscript, the blood flow trace through the aortic orifice was recorded at the peak systole for evaluating the direction of inlet flow. It is observed that the inlet flow direction beyond the aortic orifice is not parallel to the longitudinal axis of the proximal ascending aorta, but forms an angle of 26±1 degrees. This phenomenon is also clearly visualized in **Figure I-H, I, J**. In addition, the peak systolic diameter of the aortic orifice was significantly smaller than that of the proximal ascending aorta (1.07±0.01 *vs* 1.31±0.02mm; $p<0.01$). Therefore, the systolic inlet flow stream converged and accelerated by the smaller aortic orifice reaches the relatively wider proximal ascending aorta on the side of greater curvature. Consequently, the flow along the lesser curvature moves forward at a relatively lower velocity. At the early diastole with a quick reversal of the pressure gradient between aorta and left ventricle (preceding the closure of aortic valves), it is easier for the flow with lower

forward velocity along the lesser curvature to turn its direction. The findings of the inlet flow jet off-axial direction and the diastolic retrograde flow along the lesser curvature are consistent with the observations in humans using 3D MR velocity mapping[(2)].

No retrograde flow was observed in the abdominal aorta, either the proximal (suprarenal) or distal (infrarenal) segments.

(B) Aortic flow distribution in *Ldlr*$^{-/-}$ mice with AR

In 5 *Ldlr*$^{-/-}$ mice without AR and 5 *Ldlr*$^{-/-}$ mice with AR, Doppler color flow imaging was conducted at 7 weeks after AR creation (e.g., 6 wks after high fat diet feeding and 21 wks of age). Otherwise the methods were the same as described above.

The *Ldlr*$^{-/-}$ mice without AR was similar to C57BL/6J mice in the aortic flow distribution. In the *Ldlr*$^{-/-}$ mice with AR, Doppler color flow imaging demonstrated a more asymmetrical flow velocity distribution across the lumen during systole and a consistent retrograde flow during diastole in the ascending aorta and aortic arch **(Figure II)**. In mice with severe AR, with significant increase of the systolic antegrade flow velocity along the greater curvature, the flow along the lesser curvature between the distal ascending aorta and proximal aortic arch was much lower in amplitude, and moreover started to reverse at early systole and continued to be retrograde into the diastole **(Figure II-A, B, C)**. Such flow separation with flow reversal along the lesser curvature during the mid-to-late systole was observed in normal humans in the same region[(2)] and also tended to occur in the untreated C57BL/6J mice in the present study (**Figure 1C** of the primary manuscript). In AR mice, the significantly elevated forward velocity along the greater curvature during the systole **(Figure II-D)** might facilitate the occurrence of the flow separation, causing the early flow reversal along the lesser curvature. This observation explains the dominant retrograde flow occurring during

the most systole and the whole diastole detected by pulsed Doppler from that location **(Figure II-F)**. The reason to focus on this region was that, in *Ldlr*$^{-/-}$ mice with severe AR, the plaque along the lesser curvature between the ascending aorta and the aortic arch, a naturally plaque-prone region, surprisingly decreased. It is of considerable interest to investigate further the association between the change of local flow pattern and the reversal of atherosclerotic susceptibility. In the aortic arch, the asymmetrical systolic antegrade flow distribution with higher velocity along the greater curvature but relatively uniform diastolic retrograde flow across the lumen was observed.

In the proximal abdominal aorta, Doppler color flow imaging demonstrated a parabolic and laminar flow which was consistently antegrade throughout the cardiac cycle in mice without AR. In mice with AR, the systolic antegrade flow was laminar, but with the highest velocity slightly closer to the posterior wall. The diastole flow was consistently retrograde with symmetrical velocity distribution. All results confirm the pulsed Doppler recordings from the separate locations at the same level, and exclude the involvement of turbulent (or disturbed) flow in the plaque formation in this distal aortic segment far from the origin of flow perturbation (e.g., the damaged aortic valve).

The *Ldlr*$^{-/-}$ mice in this supplemental experiment demonstrated similar effects of AR-induced flow alteration on plaque distribution as presented in the primary manuscript.

For mice with high heart rate, the time needed for constructing the Doppler color flow image might cause distorted flow visualization. With a frame rate of 70fps, the time spent for color flow imaging was about 9ms (2/3 of the total time for one frame). Considering the targeted aortic lumen was about one-third to a half of the width of the color flow sampling window, the time delay from one side to another of the vessel was less than 5ms, and therefore acceptable. Moreover, the Doppler color flow was used only for qualitative visualization of the flow direction. The image of the same structure by rotating transducer for 180 degrees showed the similar flow patterns. Most importantly,

asymmetrical flow distribution across the lumen and the local flow direction demonstrated by Doppler color flow imaging were consistent with the pulsed Doppler recording which had an excellent temporal resolution.

In summary, the aortic flow distribution visualized by Doppler color flow imaging has convincingly confirmed the local flow patterns observed using pulsed Doppler at the discrete locations in aorta in mice with normal flow dynamics and AR. Furthermore, the high spatial resolution flow distribution across the aortic lumen throughout the cardiac cycle provides important clues for explaining the observed various local flow patterns.

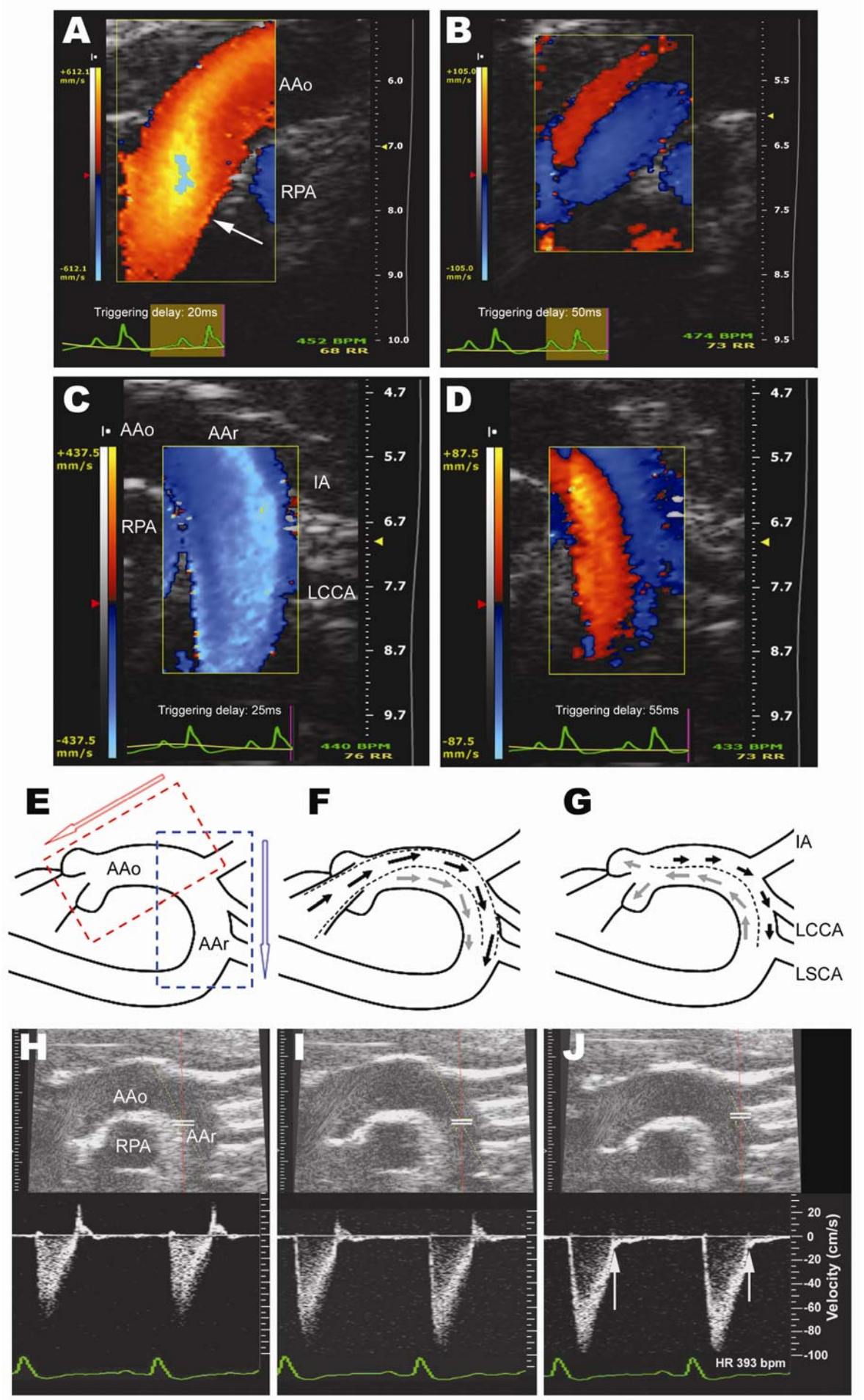

Figure I. Aortic flow distribution in C57BL/6J mice. **(A)** The Doppler color flow image frame at peak systole showing the inlet flow (red) through the aortic orifice (arrows) and the higher velocity (the area with aliasing and orange color) along the great curvature and the lower velocity along the lesser curvature of the ascending aorta (AAo). **(B)** The frame at early diastole showing the retrograde flow (blue) along the lesser curvature of the AAo and also in the aortic sinuses, but with the flow along the greater curvature still moving forward (red). **(C)** The frame at peak systole showing the antegrade flow in the aortic arch (AAr) with the higher velocity along the greater curvature and the lower velocity along the lesser curvature. **(D)** The frame at early diastole showing the retrograde flow (red) along the lesser curvature, but with the flow along the greater curvature still moving forward (blue). In panel **E**, the red open arrow and rectangle represent the direction of transducer and the orientation of Doppler color flow imaging window relative to AAo for the panels **A** and **B**. The blue open arrow and rectangle represent the direction of transducer and the orientation of Doppler color flow imaging window relative to AAr for the panels **C** and **D**. **(F)** and **(G)** illustrate the flow dynamics at peak systole and early diastole, respectively. **(H), (I)** and **(J)** are Doppler flow spectra recorded along the lesser curvature, at the middle lumen and along the greater curvature in the AAr, respectively. Arrows in **J** indicate the dividing point between the systole and diastole. IA: inominate artery; LCCA: left common carotid artery; LSA: left subclavian artery; RPA: right pulmonary artery.

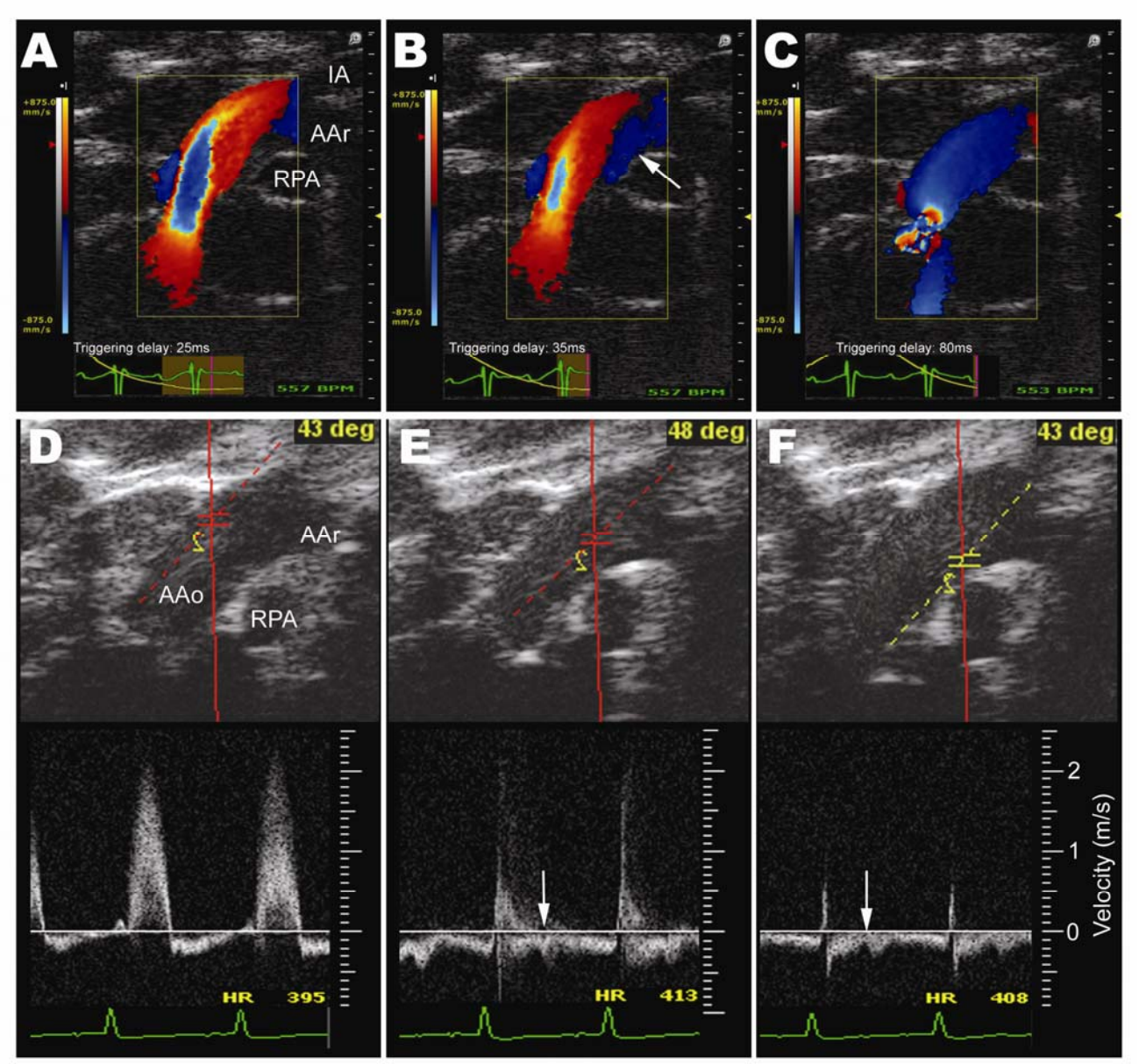

Figure II. Flow distribution in the distal AAo in a *Ldlr*$^{-/-}$ mouse with AR. **(A)** A peak systolic Doppler color flow image frame showing the inlet flow through the aortic orifice with the higher velocity along the great curvature and the lower velocity along the lesser curvature. **(B)** The frame shortly after peak systole but before diastole (which starts 50-55ms after peak R wave with a cardiac cycle of 108ms) showing the reversal flow (blue indicated by arrow) along the lesser curvature, when the flow along the great curvature is still moving forward (red). **(C)** The frame at mid diastole showing retrograde flow (blue) in the whole AAo. **(D), (E)** and **(F)** are Doppler flow spectra recorded along the greater curvature, at the middle lumen and along the lesser curvature in the distal

AAo, respectively. Arrows in **(E)** and **(F)** indicate the dividing point between the systole and diastole. Along the lesser curvature the negative waveform was recorded from the middle to late systole **(F)**, confirming the retrograde flow visualized in **(B)**. See previous figures for abbreviations.

II. Aortic diameter measurements and leukocyte count in C57BL/6J mice with AR

To evaluate the changes in aortic diameter caused by AR, M-mode recording was made at the levels of the proximal ascending aorta (L1) and the proximal abdominal aorta (L6) in five C57BL/6J mice with AR and four sham-treated control mice one week post catheterization (15 weeks of age). The end-systolic and end-diastolic diameters were measured (**Table I**). The extent of AR in these C57BL/6J mice was comparable to that in the *Ldlr*$^{-/-}$ mice with AR presented in the primary manuscript. At the proximal abdominal aorta, the calculated end-systolic cross-sectional area in the AR mice was 37% larger than the corresponding value in the control mice, but the end-diastolic cross-sectional area was similar between two groups. Within AR mice, the cross-sectional area of the abdominal aorta at end-systole was 72% larger than that at end-diastole. The results demonstrate an augmented systolic expansion of the aorta in AR mice, which is most probably due to the increase of the systolic antegrade flow for offsetting the diastolic flow reversal and maintaining the blood perfusion to limbs and viscera.

The total blood leukocyte count measured in the same mice at 8 weeks post catheterization did not show any significant difference between two groups (**Table I**). Therefore, the AR-induced cardiac remodeling and the possible consequence such as the reduced blood perfusion to distal organs did not result in any change in the leukocyte level in these normocholesterolemic C57BL/6J mice.

Table I. The aortic diameter measurements and total blood leukocyte count in C57BL/6J with AR (mean±SEM).

Parameters	**Control group (n=4)**	**AR group (n=5)**
TVI of diastolic flow in AbAo (cm)	0.70±0.09	-0.53±0.10**
Proximal ascending aorta (L1)		
ESD (mm)	1.37±0.04	1.72±0.05**
EDD (mm)	1.25±0.04	1.32±0.03
Proximal abdominal aorta (L6)		
ESD (mm)	1.05±0.04	1.23±0.03**
EDD (mm)	0.93±0.03	0.94±0.03
Total blood leukocyte count ($x10^6$/ml)	8.7±3.8 (n=3)	9.8±3.7 (n=4)

AbAo: abdominal aorta; EDD: end-diastolic diameter; ESD: end-systolic diameter; TVI: time-velocity integral.

References

1. Foster FS, Mehi J, Lukacs M, Hirson D, White C, Chaggares C, Needles A. A new 15-50 MHz array-based micro-ultrasound scanner for preclinical imaging. Ultrasound Med Biol. 2009;35:1700-1708.
2. Bogren HG, Mohiaddin RH, Kilner PJ, Jimenez-Borreguero LJ, Yang GZ, Firmin DN. Blood flow patterns in the thoracic aorta studied with three-directional MR velocity mapping: the effects of age and coronary artery disease. J Magn Reson Imaging. 1997;7:784-793.